Multiscale modelling of radiation damage and phase transformations: The challenge of FeCr alloys

Lorenzo Malerba [a,*], Alfredo Caro [b], Janne Wallenius [c]

[a] Nuclear Materials Science Institute, SCK CEN, Boeretang 200, B-2400 Mol, Belgium
[b] Chemistry, Materials and Life Sciences Directorate, Lawrence Livermore Nat. Lab., Livermore, CA 94550, USA
[c] Department of Nuclear and Reactor Physics, KTH, AlbaNova University Centre, 10691 Stockholm, Sweden

ARTICLE INFO

ABSTRACT

We review the experimental evidence of the non-monotonic behaviour of FeCr alloys versus Cr content, particularly under irradiation (ordering versus segregation tendencies, microstructure and phase evolution, hardening and embrittlement), together with the theoretical efforts done at the electronic and atomic level to interpret them. We summarize the achievements of the two interatomic potentials developed for this system and perform a careful scrutiny of their limitations. We emphasise the difficulties related to the study, at the atomic-level, of concentrated alloys and propose routes to overcome them. Finally, we advance some opinions regarding the crucial points that deserve further investigation in order to fully understand this important binary alloy, at the basis of the steels for current and future nuclear applications.

1. Introduction

Ferritic alloys, i.e. Fe-based alloys with a body-centred-cubic (bcc) structure, are long known to be highly resistant to radiation effects, such as swelling and damage accumulation, particularly compared to austenitic alloys (Fe-based alloys with face-centred-cubic, fcc, structure) [1-6]; in addition, high chromium contents are known to provide good resistance against corrosion [7]. For these reasons, high-Cr ferritic/martensitic steels, possibly strengthened with oxide dispersions, to extend their range of operating temperatures, and/or modified in their composition, to reduce the expected post-operation activity, are the leading candidate structural materials for key components in most future nuclear energy options [8-10].

Despite the expected superior properties of these steels under irradiation and against corrosion, their prolonged exposure to fast neutron fluxes and aggressive coolants in operation will unavoidably reduce their capability of withstanding the applied loads. In order to guide the design of the plant and guarantee its safe operation, a precise knowledge of the response offered by these steels to neutron irradiation in aggressive environments is thus needed. In addition, their composition should be optimised to provide the best performance. Extensive neutron irradiation experiments on a number of candidate steels, in conditions as close as possible to those expected in operation, are necessary for this purpose and are ongoing worldwide. However, these experiments are highly expensive, both in terms of time and resources, and the real operating conditions cannot be fully reproduced in any existing irradiation facility. The development of reliable models capable of guiding the designers and in synergy with the experimenters is therefore nowadays recognised to be of high value [11].

For this reason in recent years significant effort has been put, particularly in Europe and in the USA, in atomic-level studies, with a view to developing multiscale models of the response to irradiation of FeCr alloys [12–47], the reference model system to understand the behaviour of high-Cr steels [2,6,48–54]. These models have the ambition of deducing the macroscopic response of the material to given conditions starting from a detailed knowledge of the fundamental interactions between atoms. It is a long-term approach that bears, however, the promise of being reliable, transferable and beyond empiricism.

In this article, we review recent advances made in this direction, by pointing out the difficulties posed by the multiscale modelling of radiation damage in concentrated alloys in general, and in the FeCr system in particular, by discussing the different approaches followed to overcome these difficulties and by outlining the most urgent open questions to be addressed, as well as the outlook for the near future. In Section 2 we review the effects of Cr in Fe according to experiments and density functional theory (DFT) calculations, showing the challenges that multiscale models have to address in order to be able to account for them. In Section 3 we review recent advances in the development of interatomic potentials capable of reproducing the most important properties of the FeCr system from the atomistic point of view. In Section 4 we review

* Corresponding author. Tel.: +32 14 333090; fax: +32 14 321216.
E-mail address: lmalerba@sckcen.be (L. Malerba).

and discuss a few results obtained by applying the interatomic potentials previously presented. Finally, in Section 5 we outline open questions and outlook, and summarise in Section 6.

2. The challenge of FeCr

Experiments clearly show that the addition of Cr to Fe influences significantly the response of the alloy to irradiation and that this response is a highly non-monotonic function of the Cr content.

From the microstructural point of view, the presence of even small percentages (0.1%) of Cr in ultra-pure Fe induces enhanced nucleation of small dislocation loops of interstitial nature in the early stages of irradiation, both using neutrons at 400 and 425 °C and electrons in a range of temperatures between 200 and 500 °C, with a subsequently higher radiation-induced hardening [48,49]. This effect becomes even more pronounced for 2%Cr under neutron irradiation [48] and a significant enhancement of the loop density in electron-irradiated Fe10%Cr at 25 °C, as compared to pure Fe, has been also reported [50]. More recently, Arakawa et al. studied the thermal stability of loops in ultra-pure Fe and Fe9%Cr, finding that in the latter loops are stable up to 820 K, while they essentially disappear in the former already at 620 K [51]. On the contrary, the formation of voids appears to be suppressed by the presence of Cr in Fe, as shown for compositions ranging from 0 to 18%Cr at 400 °C, after neutron-irradiation up to about 6 dpa [52] and up to about 26 dpa [53]. As a consequence, swelling is about one order of magnitude lower in FeCr than in Fe, at the same dose [2,3,6,52,53]. More specifically, the measured swelling under irradiation decreases with the addition of small quantities of Cr, remains low for concentrations between 1% and 10% and then may increase again for higher Cr contents. Other data suggest a more complex modulation of the swelling curve versus Cr content, with a maximum at ∼9%Cr [6,54–56], which becomes particularly prominent at very high doses (140, 200 dpa) [55,56]. Unfortunately, in these experiments the materials matrix did not include any reference Fe, so it is impossible to say with certainty whether swelling in Fe would remain, in the same conditions, significantly higher than in any FeCr alloy (9%Cr thus representing a local maximum, with at least one local minimum at about 3%Cr). There are, however, reasons to believe that this is the case, as discussed in [6] and suggested by very recent data on swelling in pure Fe at high dose [57].

A remarkably non-monotonic effect of Cr concentration is also observed in the shift of the ductile-to-brittle transition temperature (ΔDBTT) in irradiated ferritic/martensitic steels. This shift is found to reach a minimum around 9%Cr [58,59], in a range of irradiation temperatures from 300 to 410 °C and for doses from 7 to 36 dpa. Such an effect, mainly deduced from Charpy test data for alloys containing between 2.25 and 12%Cr, i.e. again without the reference of alloys containing no Cr, was determined to be due to Cr and not to other elements. This result is in fact the main reason for choosing Cr concentrations around 9% in most steels proposed for nuclear applications. Recent experiments on FeCr model alloys of concentration up to 12%Cr, neutron-irradiated at 300 °C up to 1.5 dpa, have shown that radiation-induced hardening (yield strength increase, $\Delta\sigma_y$) is higher, and saturates at higher dose, than in pure Fe, the density of visible defects being insufficient to explain such an effect [60,61]. (Similar considerations in the case of Fe2%Cr were reported in [48].) Again, the dependence on Cr content is not regular: $\Delta\sigma_y$ is larger than in Fe already at low Cr concentration, remains almost independent of Cr content (or slightly decreases) up to 9% and then increases again above this critical concentration [60,61]. A similar trend can be deduced also from data provided in [52]. Unfortunately, the dose reached in the experiments from [60,61] may not be high enough to identify any minimum at 9%Cr, which would correlate with the minimum

ΔDBTT, while in [52] no alloy containing 9%Cr was studied; so, the consistency between irradiation-induced hardening and embrittlement data versus Cr content remains unclear. This point will be further discussed in Section 5.2. However, the non-monotonic influence of Cr content on mechanical property changes after irradiation appears to be a fact, despite early data suggesting a simple linear correlation [62].

The increase of radiation-induced hardening and embrittlement above ∼9%Cr is qualitatively understandable in terms of radiation-enhanced (and maybe also radiation-induced) precipitation of the coherent, Cr-rich α′ phase [63–66]. As a matter of fact, high-Cr steels containing more than 12%Cr are long known to harden and embrittle after thermal ageing (so-called 475 °C, or 885 °F, embrittlement) [67–72]. Searching for the reason for this initially 'mysterious' effect [67] led to the identification of the existence of the miscibility gap between Fe-rich (α) and Cr-rich (α′) bcc phases [68,69], that characterises the currently accepted FeCr phase diagram. Yet, it is not equally apparent how to rationalize the overall higher radiation-induced hardening in FeCr compared to pure Fe, not matched by the visible defect density [48,60,61], and even less to understand the reasons of the ΔDBTT (local?) minimum at ∼9%Cr, i.e. its increase not only *above*, but also *below* this concentration, and how this behaviour correlates with hardening data.

Even in the absence of irradiation, the FeCr system exhibits a number of peculiarities. Resistivity measurements and neutron scattering studies on well-annealed alloys revealed the existence, at about 700 K, of an inversion of the sign of the short-range order (SRO) parameter from negative (at 5%Cr) to positive (at 15%Cr), the zero crossing occurring at about 10%Cr [73]. This is equivalent to saying that in Fe5%Cr solute atoms tend to be surrounded by Fe atoms, an effect obtained e.g. by being as far apart from each other as possible, with possible onset of long-range order. In Fe15%Cr, on the contrary, they tend to be surrounded by other Cr atoms, i.e. to segregate, consistently with α′ precipitation. Only Fe10%Cr is suggested to correspond to an ideal solid solution, on average (this point is further discussed below). The same effect has been seen in more recent Mössbauer and X-ray studies, which revealed that, in Fe alloys containing 4, 9 and 16%Cr, solute atoms showed a tendency to prefer, as first neighbours, respectively, Fe atoms, any atom, or atoms of the same species, [74]. Interestingly, the same result for the three alloys was observed both after being thermally aged at 700 K and electron-irradiated at 370 K [74]. Similar investigations [75] showed that, after 10 h annealing at 773 K, alloys containing 9%Cr still exhibited ordering, while in 13%Cr alloys the formation of the α′ phase was detected. Equivalent results were obtained after irradiating with electrons at 573 K [75].

An explanation for the origin of this negative value and inversion of the sign of the SRO came recently from DFT calculations. Studies performed with different DFT methods and in different approximations show that the mixing enthalpy of random or quasi-random FeCr solid solutions, as well as partially ordered alloys, is negative below a critical concentration and becomes positive above it [12,22,26,27,32,40,76,77]. Although quantitative differences exist depending on the used DFT approximation (the critical concentration shifts between 4 and 10%Cr, the depth of the negative well changes, and the maximum in the positive part changes, too), this result is in qualitative agreement with the aforementioned experiments. The analysis of the DFT results provided also a physical explanation for this effect, in terms of electron band and magnetic properties of Fe and Cr [26,27]. The single Cr atom has a negative heat of formation and thus prefers to be surrounded by Fe atoms because of a lowering of the density of states at the Fermi level, i.e. of the total energy [26]. In addition, in their respective ground-states pure Fe is ferromagnetic and pure Cr can be described as antiferromagnetic [27,78]. Thus, if a single Cr atom is inserted in the Fe matrix, its magnetic moment will be antiparallel

to that of the surrounding Fe atoms. However, if a second Cr atom is introduced nearby, a situation of 'magnetic frustration' is produced, because either Cr atom tends to have its magnetic moment antiparallel to both that of the surrounding Fe atoms and to that of the other Cr atom. Since this is impossible, when many Cr atoms are close to each other in Fe different magnetic configurations can result from the competition [27], but in practice the energetically most favourable situation is obtained when the Cr atoms are distributed sufficiently far from each other to avoid magnetic frustration, i.e. by ordering the alloy. When, however, the concentration of Cr is high enough, Cr–Cr interactions cannot be avoided, leading to a positive formation enthalpy, i.e. to a tendency to segregate. Additional insight has been obtained very recently, pointing out that the negative short-range order found for sufficiently low Cr concentrations is not only the result of a pure repulsion between Cr atoms, but that, in addition, an effective long-range attractive interaction between Cr atoms seems to exist, which appears to stabilise precise intermetallic phases, endowed with long-range order, at low temperature [40]. The possible existence of a long-range ordered compound in this region has been also proposed by Nguyen-Manh and co-workers [77,79]. The importance of magnetic effects in determining the atomic distribution in FeCr alloys is further reflected in the different dependence of the Cr–Cr pair repulsion energy on distance found by DFT calculations in defect-free alloys and in the presence of self-interstitials [32]: in the latter case the

magnetic moments are locally reduced in absolute value, so the magnetic energy contribution is somewhat screened and, as a consequence, the Cr–Cr pair repulsion energy is reduced compared to the defect-free alloy (see Fig. 7 in [32]). Further evidence on the link between Cr distribution and magnetic properties in FeCr alloys has been provided by directly comparing experiments and DFT calculations in [39].

Note that the aforementioned theoretical and experimental results concerning negative mixing enthalpy and order are not correctly reflected in the standard FeCr phase diagram, as reported in reference handbooks [80], or as obtained for example from the Calphad database [81,82]. In Fig. 1 we show a portion of the Calphad solid phase diagram for FeCr. In it, the miscibility gap at low temperature, when Fe is ferromagnetic, appears to be fairly symmetric and to have a regular behaviour, i.e. very low solubility in both terminal solutions, going to zero at 0 K. The experimental points taken from the references mentioned in the figure and the evidence of negative mixing enthalpy from DFT calculations provide, however, solid arguments to state that the standard FeCr phase diagram is incorrect at low temperature and low Cr content. Other well-known peculiarities of the FeCr phase diagram, in no contradiction with theory, are: the appearance of a σ-phase at high temperature and at concentrations close to 50%Cr (which makes the α–α′ miscibility gap metastable above a certain temperature, see Fig. 1); the occurrence of spinodal decomposition at the centre

Miscibility gap boundary
△ ref. a, thermal ageing
□ ref. b, neutron irradiated steels
○ ref. c, low T e-irradiation & high T thermal ageing
◇ ref. d, proton-irradiation, precipitates no more dissolved
▬ ref. e, thermal ageing, atom probe, spinodal decomp.
▬▬ ref. f, thermal ageing, atom probe, spinodal decomp.

Order or precipitate dissolution observed
✕ ref. g, thermal ageing
✳ ref. c, low T e-irradiation & high T thermal ageing
+ ref. d, proton-irradiation, annealed radiation induced precipitates dissolve

Precipitation observed
▲ ref. d, proton-irradiation, annealed radiation induced precipitates not dissolved
● ref. c, low T e-irradiation & high T thermal ageing
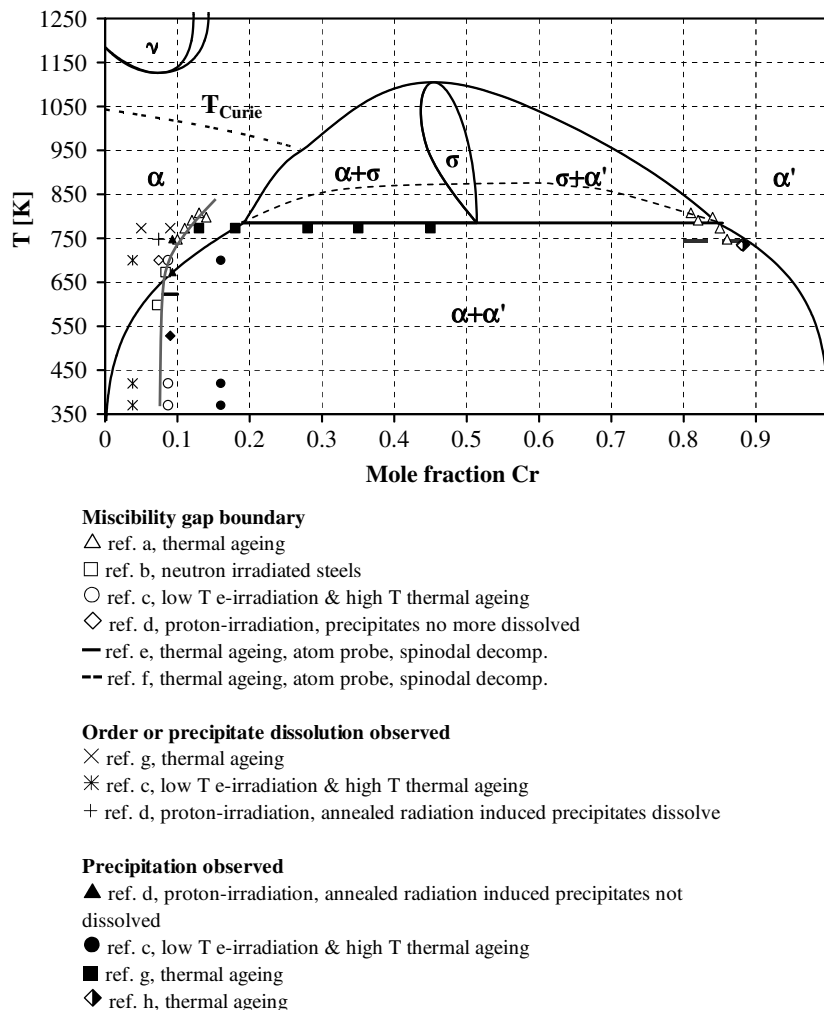■ ref. g, thermal ageing
◆ ref. h, thermal ageing

Fig. 1. Portion of the FeCr phase diagram according to Calphad and low temperature experimental data from [83] (ref. a), [65] (ref. b), [74] (ref. c), [84] (ref. d), [85] (ref. e), [86] (ref. f), [75] (ref. g) and [87] (ref. h). In the figure, the metastable closure of the α–α′ miscibility gap is also shown (dashed grey line).

of the α–α' miscibility gap; and the existence of a γ-phase loop at low Cr concentration and high temperature. For a more thorough review and discussion of these features see Ref. [30].

DFT calculations have been also performed to study in detail the interaction between Cr atoms and point-defects in Fe [21,22, 32,38]. These studies show that, while the interaction energy between Cr atoms and vacancies in Fe matrix is negligible (the vacancy-Cr binding energy is 0.057 eV at first and 0.014 eV at second nearest neighbour distance [32]: a value that excludes the possibility that Cr atoms are dragged by vacancies), self-interstitials in different configurations interact rather strongly with Cr atoms. The mixed FeCr $\langle 110 \rangle$ dumbbell is stable (while the CrCr $\langle 110 \rangle$ dumbbell is not) and, more importantly, both FeFe and FeCr dumbbells can be attracted, or repelled, by a Cr atom nearby. This is illustrated in Table 1, where a small number of configurations and their corresponding binding energies are indicated (a positive binding energy means attractive interaction). Recent DFT calculations show that the influence of a nearby Cr atom on the migration energy of the self-interstitial is also significant, in the sense of lowering it [88].
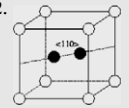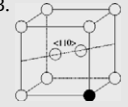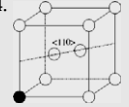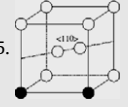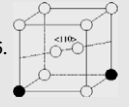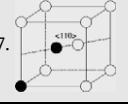
In agreement with the picture stemming from these DFT calculations, isochronal annealing resistivity recovery studies in dilute FeCr alloys showed that the recovery stage I_E, associated with the onset of single self-interstitial migration, shifts to lower temperature with increasing Cr concentration, thereby suggesting the stability of the mixed dumbbell and its capability of migrating with somewhat lower energy than in pure Fe [89,90]. On the other hand, similar studies in concentrated FeCr alloys have been interpreted in terms of the existence of trapping configurations for the dumbbell, involving more than one Cr atom, capable of suppressing recovery stage I_E and of producing peaks at higher temperatures [89]. These peaks, that may appear at temperature even higher than the one associated with vacancy migration onset (essentially invaried in Fe and FeCr alloys) [91], can be explained in terms of self-interstitial detrapping from configuration traps with energies as high as 0.5 eV [45]. Although interpreted in terms of mixed dumbbell instability when published, also other resistivity recovery experiments in concentrated alloys [92,93] suggest stage I_E suppression in FeCr and detrapping at higher temperature [45]. It is, of course, rash to extrapolate a few results of DFT calculations in the presence of only one or two Cr atoms, in an otherwise perfectly pure Fe matrix, to explain trapping effects in concentrated alloys; yet, the qualitative consistency is worth mentioning. In addition, proper allowance for the effects of a high local concentration of Cr in DFT studies has been recently attempted [38]. The results show that, when Cr atoms are monoatomically dispersed (i.e. in configurations characterised by a certain degree of order), the strength of the nearby-Cr/dumbbell interaction is significantly enhanced, by a factor two or more, once again suggesting the existence of trapping configurations affecting the mobility of self-interstitials in concentrated FeCr alloys, when compared to Fe, in agreement with the resistivity recovery studies cited above.

On the other hand, the negligible interaction between Cr atoms and vacancies found in DFT calculations is also consistent with a number of results found in the literature. Using an all-electron calculation method, Demangeat had already estimated long ago the vacancy-Cr binding energy in Fe to be lower than 0.089 eV [94]. Muon spin rotation measurements by Möslang and co-workers confirmed this theoretical result, by reporting a binding energy below the resolution of the method, i.e. less than 0.1 eV [95]. Finally, positron annihilation measurements associated with resistivity recovery experiments reveal that the onset of vacancy migration (recovery stage III) in pure Fe and Fe–Cr alloys up to 15%Cr is the same [93,96], suggesting negligible effect of Cr on the effective migration energy of the vacancy, even for high concentration. Indirectly, this also excludes the possibility of vacancy-trapping by Cr atoms, contrary to what is seen to occur in the case of self-interstitials. The absence of significant interaction between vacancies and Cr atoms, even in concentrated alloys, where phase separation occurs, has been moreover postulated to explain the experimentally observed existence of large zones denuded of α' precipitates surrounding voids [2]. These denuded zones would arise because of preferential exchange of Cr atoms with vacancies migrating towards the voids, with consequent preferential flow of Cr atoms in the opposite direction, this *de facto* representing a possible mechanism of radiation-induced precipitation. Such a mechanism would not be possible if Cr atoms were sufficiently strongly bound to a vacancy to trap it or to be dragged by it. Having said that, Cr is known to diffuse in bcc-Fe somewhat faster than Fe itself [97–100] (consistently, DFT calculations predict a barrier for Cr atom exchange with a vacancy in Fe about 0.15 eV lower than the corresponding barrier for the Fe atom [32]). The diffusion coefficient of Cr in Fe is also found to depend on Cr concentration [97–100], especially at high temperature [100]. Thus, in principle some effect of Cr concentration on the effective migration energy of vacancies can be expected, particularly at high temperature and Cr concentrations.

Thus, the results of DFT calculations concerning single-defect/Cr interaction appear to be qualitatively and, when a comparison is possible, also quantitatively in agreement with experiments, providing then a key for their interpretation. Another result of DFT, that cannot be directly compared with experimental measurements, but is equally important and has measurable consequences (see Section 4.2), is that the interaction between Cr atoms and $\langle 111 \rangle$ crowdions is strongly attractive and also long-ranged, as illustrated in Fig. 2. This strong interaction participates to further define the picture, valid for FeCr alloys, of strong interaction of solute atoms with self-interstitials, though much less with vacancies. The crowdion is not the ground state configuration for the single-interstitial in Fe and is unlikely to appear even at high temperature [101–103], thus in reality *single* crowdions will hardly ever interact with Cr atoms. Nonetheless this result suggests that the crowdion configuration may be stabilised by the presence of high concentrations of Cr and this has been indeed observed in simulations performed in Ref. [45]. This fact may have important consequences, not only on further lowering the migration energy of the single self-interstitial at high temperature, by making the crowdion configuration accessible [32], but also because crowdions are the

Table 1
Binding energies of different Cr-SIA configurations according to DFT [32] and the 2BM potential [19,20,45]

Configuration	DFT	2BM	Configuration	DFT	2BM
1.	0.08	0.14	2.	−0.42	−0.29
3.	−0.08	0.16	4.	0.05	0.11
5.	−0.04	-0.05	6.	0.15	0.19
7.	0.15	0.04	8.	−0.21	−0.07

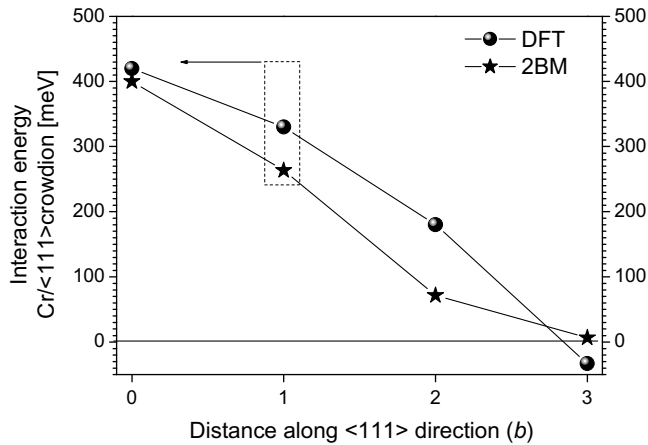All values are in eV. Positive values denote attractive interaction.

Fig. 2. Interaction energy Cr atom/crowdion when the Cr atom is located at different distances (in terms of first nearest neighbour distance, b) along the $\langle 111 \rangle$ direction, according to DFT [32,45] and as calculated using the 2BM potential [45]. Note that the Cr location at one b from the centre of the crowdion can only be achieved by fixing the Cr atom, as otherwise the Cr atom would spontaneously become the centre of the crowdion (this is the meaning of the box and the arrow).

building blocks for self-interstitial clusters of sufficiently large size in Fe alloys [103,104]. A strong interaction between crowdions and Cr atoms is thus likely to translate into a strong effect of Cr atoms on the mobility of self-interstitial clusters and dislocation loops (see Section 4.2). In addition, the stabilisation of crowdions and loops due to Cr atoms is in line with the aforementioned observed higher stability of loops in FeCr alloys compared to Fe [51], as well as higher density of them [49,50].

To summarise this section, experiments show that the presence of Cr influences the response of a ferritic(/martensitic) alloy to irradiation, but the dependence of this response on Cr concentration is non-monotonic and therefore difficult to rationalize. DFT calculations provide important indications and physical explanations concerning phase stability and Cr/defect interaction, in qualitative and also quantitative agreement with experiments. The DFT results allow, therefore, qualitative speculations to be made about the behaviour of FeCr under irradiation. Together with experiments, they indicate that Cr atoms will tend to redistribute themselves according to thermodynamic driving forces that, mainly due to magnetic reasons, change direction depending on the Cr content (ordering/clustering), with direct consequences on the mechanical properties of the material (α' precipitation and subsequent embrittlement). Self-interstitials interact strongly with Cr atoms, with two consequences: they participate, together with vacancies, to determine the way Cr redistributes under irradiation (thereby determining for example whether radiation enhanced, or induced, precipitation phenomena can appear or not) and, in turn, the way Cr is distributed influences their migration properties and, therefore, the microstructure evolution (kinetics of formation of defect clusters, loops, voids, their density, their size distribution,...). The development of quantitative models capable of allowing for these combined effects is highly challenging and DFT studies are presently possible only for systems of very limited size (hundreds of atoms at the most) and can hardly be used for dynamic studies. One way, possibly the only one, of extending DFT to larger length- and time-scales is to produce empirical interatomic potentials capable of grasping at least the most important features of the FeCr system revealed by first principle calculations and experiments. The next section reviews and discusses the approaches hitherto used, with a certain degree of success, to face this problem. The following one shows examples of their applications and of how they have enhanced our level of understanding of the behaviour of FeCr alloys under irradiation.

3. Interatomic potentials

The first challenge for the development of empirical interatomic potentials for the FeCr system has been the correct reproduction of the change of sign of the mixing enthalpy curve, as this involves the introduction of an explicit or implicit dependence on concentration for the sign of the interactions [16,17,37]. This task was soon realised [17,105] to be out of the scope of the traditional embedded-atom method (EAM) [106] or of the functionally equivalent second-moment tight-binding approximation (2MTBA) [107] and to call for either modifications of this formalism or the development of a totally new formalism.

In the EAM formalism, the total energy of a system of N atoms, whose type can be different and is denoted by α or β, can be written as:

$$E = \sum_i^N \left[F_{\alpha i} \left(\sum_{j \neq i} \rho_{\alpha i, \beta j}(r_{ij}) \right) + \frac{1}{2} \sum_{j \neq i} V_{\alpha i, \beta j}(r_{ij}) \right]. \tag{1}$$

Here F is the so-called embedding function: a functional of pairwise functions of the interatomic distances, each representing the electronic density contribution due to the surrounding atoms on the central one; V is the pairwise energy contribution. Two modifications of this formalism have been proposed to fit a sign-changing mixing enthalpy, both focused on the proper fitting of the cross FeCr interaction only, and otherwise using for the pure elements already existing potentials. (In both cases the same pure element potentials have been adopted, namely the EAM-type FeFe potential by Ackland et al. [108], developed using the methodology proposed and applied already in [109], and a slightly modified version of the 2MTBA CrCr potential developed by Wallenius et al. [17]; both are state-of-the-art interatomic potentials for these two elements).

In one of the two modifications [20], after renormalising the embedding function for the pure elements to make its contribution to the mixing enthalpy negligible, an explicit dependence on concentration is introduced, by multiplying the pair interaction term times a function $h_{\alpha i \beta j}(x^\beta)$:

$$E = \sum_i^N \left[F_{\alpha i} \left(\sum_{j \neq i} \rho_{\alpha i, \beta j}(r_{ij}) \right) + \frac{1}{2} \sum_{j \neq i} h_{\alpha i, \beta j}(x^\beta) V_{\alpha i, \beta j}(r_{ij}) \right] \tag{2}$$

with $h_{\alpha i \beta j}(x^\beta) = h_{\beta i, j}(x^\beta) = 1$. Here x^β is the local concentration of species β, which is postulated to be given by the average at the two interacting atoms of the ratio between partial and total electronic densities:

$$x^\beta = \frac{1}{2}(x_i^\beta + x_j^\beta) = \frac{1}{2}\left(\frac{\rho_i^\beta}{\rho_i^{tot}} + \frac{\rho_j^\beta}{\rho_j^{tot}} \right), \tag{3}$$

where ρ_i^β represents the contribution to the electronic density on atom i coming from atoms of type β only, while ρ_i^{tot} is the total electronic density. The function $h_{\alpha i \beta j}(x^\beta)$ can be written in the form of a typical Redlich–Kister expansion for thermodynamic functions (Calphad methodology) [82,110], with parameters fitted to reproduce closely the given reference mixing enthalpy curve. In principle, any shape of such curve can be reproduced and in this case the DFT mixing enthalpy data from [12] were used. The only deviations will be the consequence of relaxation effects (largely negligible in FeCr, as the two types of atoms have very similar size), of the small contribution from the embedding terms and of the accuracy whereby the local atomic concentration is correctly embodied by Eq. (3). This approach will be henceforth denoted as concentration-dependence method (CDM).

In the other modification [21,22] the dependence on concentration is introduced in an indirect way, following a somehow opposite route, i.e. by working on the embedding part, rather than on the pairwise potential. Namely, considering that not only *d*-band electrons, but also *s*-band electrons participate in defining the energy of a transition metal alloy [21,111], two separate embedding functions are introduced, one for each band, as well as correspondingly separate density functions:

$$E = \sum_i^N \left[F_{\alpha i}^d \left(\sum_{j \neq i} \rho_{\alpha i, \beta j}^d(r_{ij}) \right) + F_{\alpha i}^s \left(\sum_{j \neq i} \rho_{\alpha i, \beta j}^s(r_{ij}) \right) + \frac{1}{2} \sum_{j \neq i} V_{\alpha i, \beta j}(r_{ij}) \right].$$

(4)

The concentration dependence is here contained in the *s*-band mixed electronic density (no *s*-band contribution is assumed in the case of the pure elements) and in practice the presence of the second embedding function provides sufficient degrees of freedom to fit closely any reference mixing enthalpy curve, as in the case of the CDM. This approach will be henceforth denoted, for obvious reasons, as *two-band method* (2BM). Of the two potentials fitted with this formalism in Ref. [19], only results obtained with the one whose parameters are therein denoted as 'VASP' will be mentioned here. This potential was fitted to the mixing enthalpy data provided in [26], obtained using the VASP code [112–114]. It is important to note that, despite the apparent differences, it can be demonstrated that CDM and 2BM are mathematically equivalent [115].

Fig. 3 shows that the mixing enthalpy curves at 0 K produced using both the CDM and the 2BM potentials fit closely the reference DFT data-points in the low Cr concentration region. In particular, both reproduce the mixing enthalpy change of sign. In the high Cr region the CDM still follows its reference data, while the 2BM deviates from its own and provides a symmetrical mixing enthalpy, with negative values also on the Cr-rich side. The latter was a deliberate choice, not supported by DFT, whose consequences are shortly discussed in Section 4.1. For comparison, on the same graph the corresponding thermodynamic function obtained extrapolating to 0 K the Calphad [82] free energy expression for ferromagnetic FeCr is shown as well. The Calphad curve is never negative and is slightly more skewed to the right, while lying much lower, than any other curve. In particular, the VASP data points are not far from the Calphad extrapolation, while the EMTO data points lie much above it. Thus, the discrepancy between DFT methods is not negligible, in fact.

For completeness we mention that a correct reproduction of the mixing enthalpy sign-change at low Cr concentrations has been obtained also using cluster expansion (CE) techniques [33]. These techniques allow the energy of an alloy to be expressed in terms of configurations of atoms on a rigid lattice, by using occupational spin variables that, in the case of a binary alloy, take the values ±1 depending on whether a certain lattice node is occupied by one species or the other [116]. A smart choice of lattice subsets (clusters) allows, by fitting the cluster expansion coefficients, the energy for any lattice configuration to be properly reproduced. The CE mixing enthalpy for a random distribution of atoms [79] is also shown in Fig. 3. It appears that the CE curve is extremely similar to the CDM curve, despite the fact that different data were used for the CE fitting, namely enthalpies for partially ordered structures, calculated with VASP in [27]. A thorough comparison between CDM, 2BM and CE, in terms of capability of predicting the thermodynamic properties of the FeCr system, is provided in [115].

We remark here that, even though magnetic effects are not explicitly accounted for in either empirical potential formalism (nor they are in the mentioned CE), implicitly at least some of them are correctly reproduced. For example, Fig. 4 shows that the Cr–Cr pair repulsion, which is the main consequence of magnetic frustration, is qualitatively, and largely also quantitatively, captured by both CDM and 2BM potentials, when compared to DFT values from Refs. [27,32]. It is noteworthy that none of these DFT repulsion energy values were used as fitting parameters for either potential. In the case of the CDM, in addition, a comparison with the formation energy of different atomic configurations obtained by DFT [27], also not used for the fitting, provided very satisfactory results [36], too.

In the fitting procedure for the 2BM potential care was taken to reproduce as correctly as possible the interaction energies between self-interstitials and Cr atoms, as predicted by the DFT calculations available at the time; in particular, the stability of the mixed dumbbell was fitted exactly [21,22]. In Table 1 and Fig. 2 some of the latest and most refined DFT values concerning Cr/self-interstitial interaction [32] are presented and compared with the predictions of the 2BM interatomic potential [45]. Although the potential was not validated on this set of values and in fact was only explicitly fitted to reproduce the mixed dumbbell stability
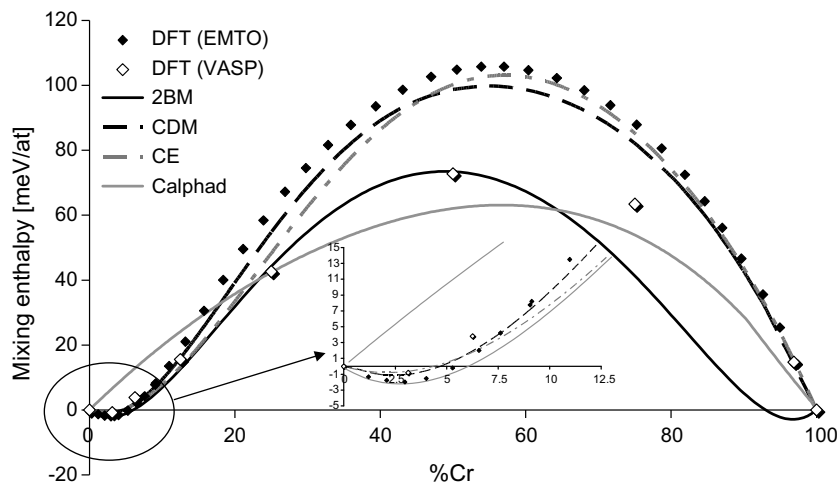

Fig. 3. Mixing enthalpy at 0 K for the FeCr system according to the CDM and 2BM potentials, as compared with the corresponding DFT reference data from [12] (EMTO) and [26] (VASP), respectively. The mixing enthalpy curve extrapolated to 0 K from the Calphad free energy and the curve deduced, for the random alloy, from a published cluster expansion (CE) fitted to DFT data [33] are also shown, for comparison. The blow-up shows more in detail the sign-changing curves in the low Cr region. The change of sign in the latter region is correctly reproduced by both potentials and by the CE.
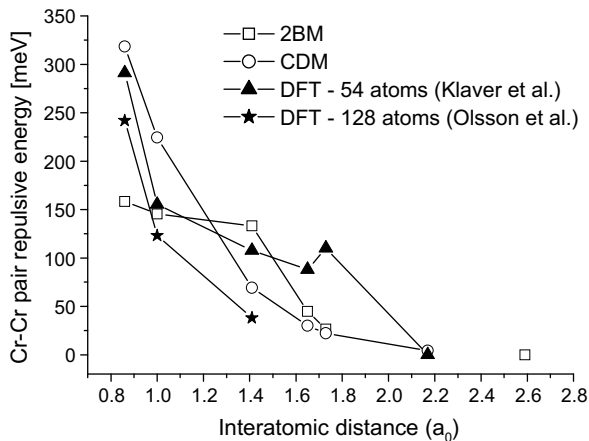
Fig. 4. Cr–Cr pair repulsive energy according to the CDM and 2BM potentials and compared with DFT data from [27] (54 atoms) and [32] (128 atoms). Note that the two sets of DFT data were obtained with the same code and approximation, so that the difference is fully ascribable to box size effects. The values obtained with the potentials correspond to a fully converged box size.

(according to earlier DFT data [22]), its predictions remain nevertheless surprisingly good, as in most cases they are qualitatively correct (same sign of the interaction energy) and in a few cases also quantitatively acceptable, although of course not all configurations are correctly reproduced. In particular, the potential succeeds in providing a satisfactory description of the Cr-crowdion interaction (Fig. 2). Thus, the 2BM potential seems adequate to assess, at least qualitatively, the atomic-level consequences of the existence of a strong Cr/self-interstitial interaction and of the stability of the mixed dumbbell. A new version of the CDM potential, that also provides a stable mixed dumbbell, has been recently developed, but it is still being tested and is not yet published.

In the following section, we review some results obtained with the CMD and 2BM potentials that reveal, at the same time, their potentialities and limitations and, more in general, the difficulty of modelling concentrated alloys from an atomistic perspective. Previous, separate reviews can be found in Refs. [35–37].

4. Application of the potentials

4.1. Thermodynamic studies

The obvious computational methods to study equilibrium and non-equilibrium thermodynamic properties of a system at the atomic level, given a model Hamiltonian such as an interatomic potential, are Monte Carlo (MC) simulations [117]. The Metropolis Monte Carlo (MMC) algorithm [117,118] is especially suited to drive the system towards thermodynamic equilibrium. It allows the redistribution of atomic species at different temperatures and for different concentrations to be sampled, not only in defect-free, fully coherent alloys (homogeneous nucleation of new phases), but also in the presence of lattice mismatch and extended defects, such as other crystallographies, dislocations and grain boundaries (heterogeneous nucleation). The algorithm accounts for all terms that contribute to defining the free energy difference between states (thermodynamic driving forces), within the used model Hamiltonian: not only chemical, configurational and interfacial, but also due to strain fields. The efficiency in reaching equilibrium for large systems can be enhanced by applying parallelisation techniques [119]. However, along the path towards equilibrium, the configurations visited using MMC do not represent a physical trajectory. Kinetic processes can be studied using MC techniques known as *dynamic* or *kinetic* MC (KMC) [120], but in this case additional

approximations have to be introduced and typically these methods assume rigid lattices [121,122]. As such, they cannot treat heterogeneous nucleation problems and cannot allow for vibrational entropy effects. They can, however, produce time evolution sequences, under the action of simplified driving forces and mobility rules, corresponding to the effect of physical diffusion mechanisms, and can therefore be used to trace the diffusion of species and defects under, for example, irradiation, in conditions that may turn out to be quite apart from thermodynamic equilibrium. They are therefore suitable, in principle, to study coherent precipitation and segregation, both under thermal ageing and irradiation [121], within the stated limitations. In the specific case of FeCr alloys, which are coherent in the whole range of concentrations and temperature of interest for most applications, the kinetic MC limitations represent a problem only in a reduced number of cases. When these techniques are applied to study phenomena at the atomic level, it has become customary to refer to them as atomistic kinetic MC (AKMC) [121], to discriminate from other approximations where atoms are not explicitly treated (object KMC [123]). This is the denomination adopted here, too.

MMC simulations have been extensively performed using the CDM potential, while mainly AKMC simulations (using the scheme described in Ref. [122]) have been carried out using the 2BM potential. In this section we briefly report about the results obtained.

Homogeneous precipitation in FeCr has been studied with the CDM at 50%Cr (within the spinodal) and at 15%Cr, inside the miscibility gap, at 750 K [36]. The results at 15%Cr show that, due to the Cr–Cr pair repulsion (Fig. 4), a fairly large critical size has to be reached for the nuclei to become stable and, as is to be expected from coherency and small size misfit, the most favourable shape is spherical. Concerning nucleation and growth decomposition mechanisms, the concentration in the α' phase is always the equilibrium one which, for this potential, at the chosen temperature, is 99%Cr. Inside the spinodal, on the other hand, the phase separation occurs via continuous composition changes until, finally, the typical interconnected structure is obtained.

AKMC studies conducted using the 2BM potential at 673 K with 11.8%Cr allowed the stages of nucleation, growth and coarsening to be clearly distinguished as a function of time [43], although the mean size of the precipitates in the simulation was eventually smaller, and the density higher, than in experiments on steels [64,65]. Similar simulations at 740 K with 10% and 32%Cr showed precipitation via nucleation and growth in one case and spinodal decomposition in the other [21,22]. The main qualitative difference between 2BM and CDM is that the concentration of Cr in the α' is 99% with the latter and about 80–90% with the former. The main reason for this discrepancy, as further discussed in Section 5.1, can be quantitatively traced back to the different shape of the mixing enthalpy curve at 0 K (Fig. 3) [115]. Consistently with this reasoning, the CE expansion method of Ref. [33] also predicts a composition of 99%Cr. Experimentally, the composition of the α' phase at the mentioned temperature ranges between 85 and 95%Cr [64,65,83,86,87] (see also Fig. 1). Overall, the main point made here is that MC simulations with both potentials reproduce in a reasonable way the α' precipitation in FeCr alloys, including spinodal decomposition.

MC simulations aimed at reproducing the experimental results revealing the sign-change of the short-range order parameter [73–75] and at improving our understanding concerning the actual distribution of Cr atoms in FeCr alloys, have also been performed with both potentials [30,41]. An example of results at 700 K versus Cr content is shown in Fig. 5. Both potentials can reproduce the sign-change of the SRO parameter. (A similar result, with a more negative SRO parameter and a more abrupt change of sign, is obtained also with the CE method [33]; for a direct comparison of the three models see [115]). The impression is that the 2BM
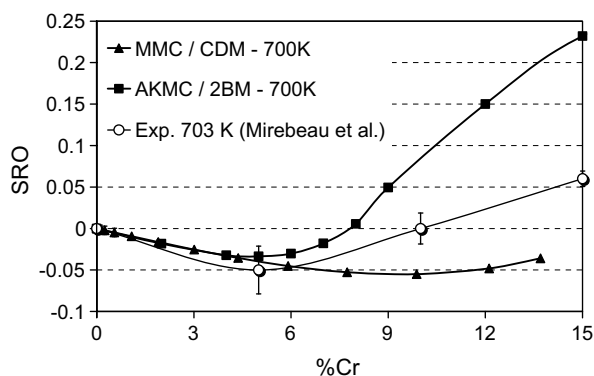
Fig. 5. Short-range order parameter (SRO) versus Cr concentration according to simulations at 700 K: (a) using an AKMC method and the 2BM potential [30] and (b) using an MMC method and the CDM potential [41]. For comparison, the corresponding experimental values from [73] are also added.

overestimates SRO in the positive region, while the CDM would underestimate it. In reality – as has been thoroughly studied and clarified in [41] – the SRO parameter measured experimentally, and calculated in Fig. 5, is in fact the average over the whole sample. The SRO parameter is negative in the α phase and positive in the α' phase. The tendency of the SRO parameter to grow after reaching a minimum and the eventual change of sign do not reflect a loss of order and the appearance of a purely random solute distribution, but only the average compensation of the negative value of the partially ordered α phase by the precipitation of Cr-rich α'. Thus, the results of simulations become extremely sensitive to the actual advancement of the phase separation process and its microstructure, in terms of size and density of precipitates, and even simulation box size. Also experimentally important differences are found, depending on the actual annealing or irradiation time [41]. Overall, both models can be said to grasp in a reliable way the effect, of magnetic origin, of the sign-inversion of the mixing enthalpy on the SRO in the Fe-rich region, at temperature of practical interest, even though neither explicitly accounts for magnetism.

The CDM was also used for the study of precipitation in presence of extended defects, namely grain boundaries and dislocations, via MMC simulations [36]. The results suggest that α' at equilibrium would precipitate away from grain boundaries and free surfaces, but would be indifferent to dislocations. These results, obtained by MMC, necessarily account purely for thermodynamic effects and disregard completely kinetics effects, which are in reality equally responsible for the microchemical evolution. Kinetics is indeed likely to play a major role in determining precipitation and segregation processes, especially under irradiation, where the possible role of crossing defect/species fluxes and diffusion via interstitialcy need to be correctly accounted for as well. Thus, these results do not mean that Cr enrichment at grain boundaries may not occur in reality, as shown in experimental studies of Fe and Cr surface atomic layers [125]. Cr rejection from free surfaces in Fe has been, however, suggested also by Geng [124], using DFT calculations, based purely on thermodynamic grounds. Interestingly, in addition, Konobeev et al. reported recently the existence of α' precipitate-free zones of about 150 nm width along grain boundaries, in 12 and 18%Cr Fe alloys irradiated up to ~25 dpa in a fast reactor [53]. However, the latter could be also an effect of kinetics, consequence of the opposed fluxes of vacancies towards grain boundaries and Cr towards the bulk [2], rather than, or in addition to, a thermodynamic effect. Finally, concerning dislocations, microstructural studies during thermal ageing reveal that α' precipitation occurs first preferentially nearby dislocations

and only later in the bulk [70]. Dislocation locking by α' precipitates has been indeed proposed as a possible mechanism to explain the sudden appearance of embrittlement after ageing at 475 °C [71]. Independently of the agreement with specific experiments, these types of simulations show that it is in principle possible, given a sufficiently reliable cohesive model, to predict the microchemical evolution of an alloy in presence of extended defects, but that kinetic effects should be also accounted for. At the moment, however, no atomistic modelling tool accounting for all effects (e.g. kinetics and extended defects such as dislocations) exists to our knowledge.

4.2. Self-interstitial studies

The 2BM potential has been extensively used to study the migration processes of self-interstitials and their clusters in FeCr alloys of different concentrations [19,24,34,42,45], using well established techniques to extract information on defect diffusion coefficients and migration mechanisms from molecular dynamics (MD) simulations (see e.g. [126]). The diffusion coefficient of the single-interstitial for different Cr concentrations calculated in this way is shown in Fig. 6(a) in the Arrhenius representation, i.e. as a function of $1/k_BT$ [45] (k_B is Boltzmann's constant, T the absolute temperature). As can be seen, the slope of the lines, which equals the effective migration energy in this representation, decreases with increasing Cr concentration and at low temperature dumbbells in FeCr appear to migrate faster than in pure Fe. It should, however, be mentioned that in many cases during the simulation the defect got trapped at a particular local atomic configuration and there it remained, immobile, for the rest of the simulation (up to 10–20 ns). Thus, these results show that single self-interstitials migrate faster in FeCr than in Fe at low temperature *so long as they are not trapped by specific local arrangements of Cr atoms*. The effective migration energy will be the result of the combined effect of a somewhat faster migration *between trapping sites* and of the *time spent in these*, which is expected to lower significantly the diffusivity prefactor. A fully correct evaluation of the effective migration energy of the single-interstitial seems therefore not to be at reach for MD simulations, as within their timeframe and lengthscale the defect will visit only a limited amount of possible atomic configurations. If one of these is a 'deep' trap, the defect will not be released within the simulation time, so the result will be of limited statistical significance; if no trap is encountered, the result will not account for traps effects. This is a clear example of the difficulty of studying, with otherwise very effective atomic-scale models, the evolution of radiation damage in concentrated alloys, particularly when defects interact strongly with solute atoms. Nonetheless, the MD results *are* in qualitative agreement with the available resistivity recovery studies in FeCr alloys [89–93] and *do provide* a key for their interpretation, as extensively discussed in [45]. In the case of diluted alloys, when the probability for the single self-interstitial to get trapped at multi-Cr-atoms configurations is negligible, the experiments suggest a decrease in the migration energy of the single-interstitial, in agreement with the simulations. When, on the other hand, the Cr concentration is high, the defect is continuously trapped and cannot annihilate, thus the experiments show a suppression of the self-interstitial migration recovery stage. In order to get an idea about the energy landscape seen by the defect while it migrates in the concentrated alloy, the distribution of statically calculated formation energies for an as-large-as-possible number of different local atomic configurations has been calculated, with the result shown in Fig. 6(b) [45]. It can be seen that the distribution is the broader, the larger the concentration, and that the peak corresponding to the mean formation energy shifts to lower values, suggesting that, on average, the effect of Cr in Fe is to trap the self-interstitial. How to define
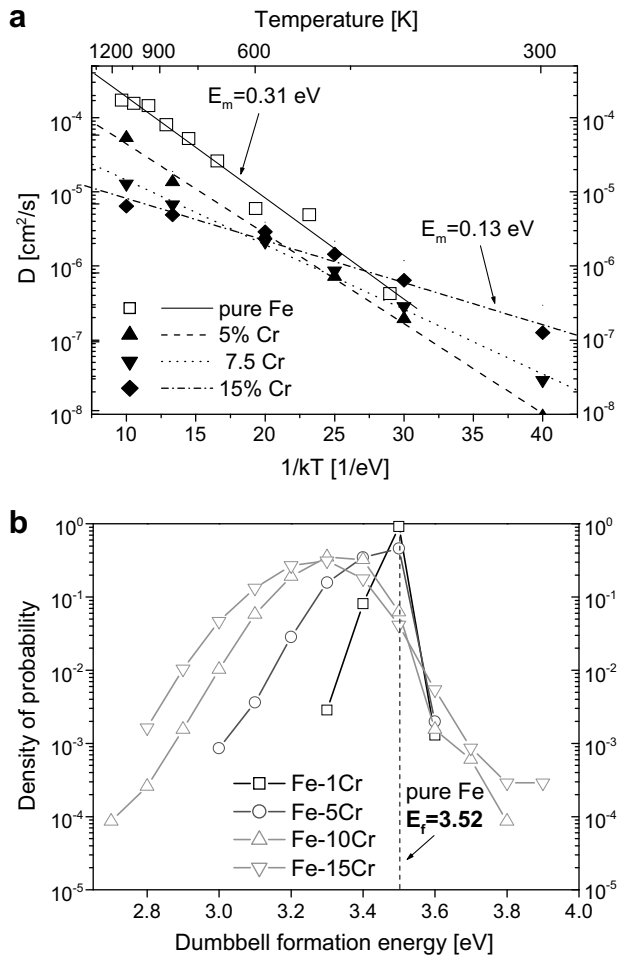
Fig. 6. (a) Diffusion coefficient of the single dumbbell in Fe and FeCr for different Cr concentrations as estimated by MD simulations with the 2BM: note the decrease of the effective migration energy. (b) Distribution of dumbbell formations energies, statically calculated using the 2BM potential for different Cr concentrations. From [45].

clusters large enough to be describable as collections of parallel $\langle 1\,1\,1 \rangle$ crowdions and produced directly in displacement cascades [14,23,24,44,127]. These are nuclei for the formation of dislocation loops and diffuse mainly via one-dimensional glide along the direction of the crowdions [103,104,128,129]. The simulations were performed in an elongated box, where the direction of motion of the cluster was the x-axis, so as to maximise the distance covered by the defect, before going through periodic boundary conditions and revisit the same configurations, for a given simulation volume. In Fig. 7 the results in the case of a 7-self-interstitial cluster at 640 K for different Cr concentrations in random alloys are summarised. This defect size can be considered the typical size for SIA clusters directly produced in cascades [127], while being the smallest perfect dislocation loop that can be created (the next one is composed by 19 crowdions, see e.g. [104]); its smallness facilitates its treatment in MD simulations and increases the number of conditions that can be explored, while remaining representative of the behaviour of larger clusters, too. The results are given in terms of ratio between the diffusion coefficient of the same cluster in FeCr and in Fe (D_n^{FeCr}/D_n^{Fe}, where n is the size of the cluster). However long the box may be, these simulations are of course affected by the same problem as in the case of the single-interstitial: within the MD timeframe and lengthscale, the defect can only visit a limited number of local atomic configurations, which do not exhaust all possibilities. Thus, the average provided by the simulation cannot be quantitatively fully accurate, even assuming that the interatomic potential is fully accurate (this problem also accounts for the rough profile obtained by showing all MD data points on the same graph in Fig. 7). Nonetheless, qualitatively the result is relevant and clearly shows that, by adding Cr to Fe, the diffusivity of self-interstitial clusters may drop by about two orders of magnitude. For clusters of larger sizes (37 and 91 crowdions) the observed reduction is somewhat less spectacular, but remains of about one order of magnitude; in addition, the maximum reduction is observed to shift to lower Cr concentrations with increasing size [42]. This reduction is of course the consequence of the strong attractive interaction between Cr atoms and crowdions mentioned in Section 2 (Fig. 2) and it is crucial to remark that the diffusivity ratio reaches a minimum (depending on size) between 3 and 10%Cr and then increases again, thereby reminding the swelling dependence on Cr content [2,6,52,53]. This non-monotonic behaviour has been rationalized within a formally simple model, which
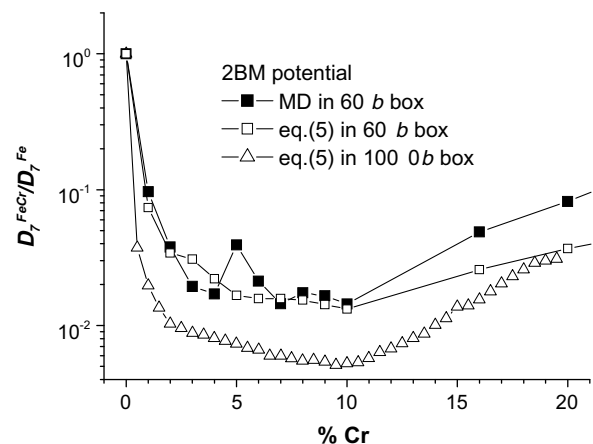
a trapping configuration and the corresponding trapping energy is not, however, clearcut, for it depends on how the reference state is chosen. The trapping energy is more of a dynamic, than static, concept: it is the energy surplus to be added to the *migration* energy in order for the SIA to be released and be able to diffuse 'freely', until it is re-trapped. Energy states such as the most frequent ones in high Cr content alloys (10, 15%Cr) will often correspond to mixed FeCr dumbbells which, as shown in Fig. 6(a), can migrate with an energy *lower* than that of the FeFe dumbbell. This happens because, so long as the SIA can migrate from one low energy configuration to another, via one single diffusion jump, the net result is long-range SIA migration, even though its formation energy is lower than in other configurations. It will be possible for the SIA to migrate 'freely' so long as, on average, at least one of the possible destinations of the single diffusion jump has energy comparable with the one where the SIA lies. Thus, trapping configurations can be defined as sufficiently unfrequent, very-low-energy states that are not likely to be connected to each other at diffusion jump distance. Based on this idea, it is possible to propose criteria to identify trapping configurations, as done in [45]. Therein, trapping energies of 0.3 eV in Fe5%Cr and of 0.4–0.5 eV in Fe10%Cr and Fe15%Cr have been estimated for the single SIA.

MD studies of the migration of self-interstitial clusters in FeCr have also been performed [19,24,25,34,42]. The study focused on

Fig. 7. Ratio between the diffusion coefficient of a 7-interstitial cluster in FeCr and in Fe for different Cr concentrations as estimated (i) by MD simulations in a $\langle 1\,1\,1 \rangle$-oriented box whose length was $60b$, (ii) by static calculations in the same box and then applying Eq. (5) and (iii) by static calculations in a longer box ($1000b$). All calculations were done with the 2BM potential. Note the decrease up to 10%Cr and the subsequent increase of the diffusivity ratio. From [34,42].

ascribes the drop in the diffusivity ratio to the time spent by the cluster in the different possible Cr configurations that trap it with binding energies E_b (assuming no influence on the migration mechanism and energy) [19,24,34,42],

$$D_n^{FeCr}/D_n^{Fe} = \exp(E_b/k_B T), \tag{5}$$

where $\langle \ldots \rangle$ indicates the average. The one-dimensional character of the migration and the long-range of the Cr-crowdion interaction (see Fig. 2) allow one to understand qualitatively that the delay in the migration will be maximum when each crowdion in the cluster, on average, interacts with one Cr atom only, a situation that will be reached at a critical Cr concentration that can be mathematically estimated [19,24,34]. Thus, the diffusivity ratio will keep decreasing up to that critical concentration. Above it, the same crowdion will start to be 'pulled' simultaneously by two Cr atoms, so the effective binding energy will decrease and, consequently, the diffusivity ratio will increase again. The other two curves in Fig. 7 correspond to estimating the diffusivity ratio using Eq. (5), after having sampled statically a number of local atomic configurations, in two simulation boxes, of different length (expressed in units of 1st nearest neighbour distances, b): one the same as in MD, the other much longer. These curves show that not only is the model embodied by Eq. (5) accurate enough to reproduce, based on static calculations, the result of much heavier dynamic calculations, but also that, by increasing the number of visited atomic configurations (longer box), the average becomes statistically more significant and the effect is that the drop in the diffusivity ratio is even more pronounced. Both dynamic and static studies coincide in showing that, as mentioned, the minimum diffusivity is reached at lower Cr concentrations for larger clusters [24,34,42]. The reduction of the self-interstitial cluster mobility with Cr content will enhance the probability of recombination with freely-migrating single vacancies, while limiting the transport of atoms from the bulk to grain boundaries and free surfaces. Consequently, the rate of formation of voids will decrease and this is equivalent, in a production-bias model framework [130,131] to a reduction in swelling. The close resemblance between the dependence on Cr concentration of cluster mobility and experimentally measured swelling [2,6,52,53] may thus not be accidental. It is also interesting to observe that, experimentally, higher doses and temperatures cause a shift of the minimum observed swelling to lower Cr concentrations [2,6], which may correlate with an average larger size of self-interstitial clusters. Finally, the local maximum swelling experimentally found at about 9%Cr for high doses [54,56] may be the consequence of the radiation-enhanced formation, at higher concentrations, of a fine dispersion of previously absent α' precipitates. MD studies with the 2BM potential have indeed shown that α' strongly repels self-interstitial clusters [34], this effect being very much in agreement with what can be deduced from DFT studies of defect formation energies in Fe, Cr and FeCr [32]. Thus, a one-dimensionally migrating cluster is expected to remain trapped between two precipitates and this may represent a different mechanism, operating at high Cr concentrations, that would also lead to an effectively reduced cluster diffusivity, thereby increasing vacancy recombination rate and decreasing swelling. Being between the ranges where two different and very effective mechanisms of SIA cluster mobility reduction operate, the 9%Cr concentration would eventually develop a (local) maximum swelling.

5. Discussion and open issues

5.1. Improvement of interatomic potentials consistent with thermodynamics

As shown, both CDM and 2BM interatomic potentials succeed in reproducing the mixing enthalpy change of sign in the Fe-rich region, depending on Cr content, that characterises the ferromagnetic FeCr systems, following the (0 K) DFT data taken as reference (Fig. 3). Also the consequences of this change of sign, namely the tendency to create order or to produce Cr-rich precipitates, are reproduced by the cohesive models at finite temperature, when these are implemented in Monte Carlo tools (Fig. 5). Similar results have been also obtained by applying the CE approach [33]. The question to be asked is, however, up to what extent these models, fitted to DFT data at 0 K, may remain thermodynamically reliable at finite temperature. Such a question has been addressed in [115], where the differences between these three models (CDM, 2BM and CE) concerning the numerical prediction of thermodynamic properties and microchemical evolution in FeCr alloys have been analysed in detail. One of the main conclusions from the cited work is that, unfortunately, there is no all-including tool to evaluate the phase diagram embodied by a given cohesive model and that, conversely, the same model, implemented in different tools (e.g. MD, or MMC accounting or not for vibrational effects, or AKMC on rigid lattice), may provide somewhat different descriptions of the thermodynamic properties of the same system. In addition, the comparison has highlighted that fitting mixing enthalpy data at 0 K is far from being a sufficient condition to guarantee the reliability of a model at finite temperature. In general terms there are, at least, two other 'ingredients' that need to be accounted for: the vibrational entropy and the stability of specific long-range ordered structures, as predicted by the model. The CDM potential has been found to embody negligible (and highly anharmonic) mixing vibrational entropy and to exhibit hardly any low energy structure; as a consequence, the free energy from this model is acceptably assessed by simply adding the configurational mixing entropy contribution to the mixing enthalpy of Fig. 3. A better evaluation can be otherwise obtained by applying a thermodynamic package recently developed and applied to a number of systems [132–134], as has been done, including SRO effects, in [135]. Conversely, the 2BM potential has been found to embody a non-negligible, largely harmonic mixing vibrational entropy (only a little in excess of experimental measurements performed in the FeCr system [136]) and to stabilise a large number of (unwanted) structures, one of which, at 50%Cr, is a ground-state. This fact makes the evaluation of the corresponding phase diagram in regular solution approximation inadequate and demands the application of more sophisticated techniques [115].

The CDM and 2BM FeCr phase diagrams (α–α' miscibility gap) in regular solution approximation are shown in Fig. 8. Despite the significant difference in the fitted mixing enthalpy curve (Fig. 3), they are similar. In particular, the closure of the gap occurs at very close temperatures and, to this regard, it is interesting to note that, in the same approximation, the phase diagram obtained from the CE from [33] is much higher, almost 3400 K [115]. This already highlights that apparently similar zero-Kelvin mixing enthalpy curves do not necessarily lead to the same phase diagram. If the effect of low energy structures is accounted for, then the closure of the gap lowers to about 1600 K according to 2BM (and CE [33]), while it remains unchanged with CDM [115]. Finally, if also the vibrational entropy contribution is included, the closure of the gap lowers to about 1000 K for the 2BM, in fair agreement with the closure of the (metastable) α - α' miscibility gap according to Calphad (Fig. 1), while the CDM prediction remains unchanged, because of the negligible vibrational contribution (the CE is a rigid lattice model, thus no vibrational entropy can be explicitly included) [115]. Even remaining in the regular solution approximation evaluation, there is still another important difference between the predictions of 2BM and CDM: the *solvus* converges to 100%Cr in the low temperature limit only in the latter case. This is of course a direct consequence of the deliberately-chosen symmetric mixing enthalpy curve with the 2BM (Fig. 3), with a negative part in the Cr-rich region, too, not supported by DFT data.
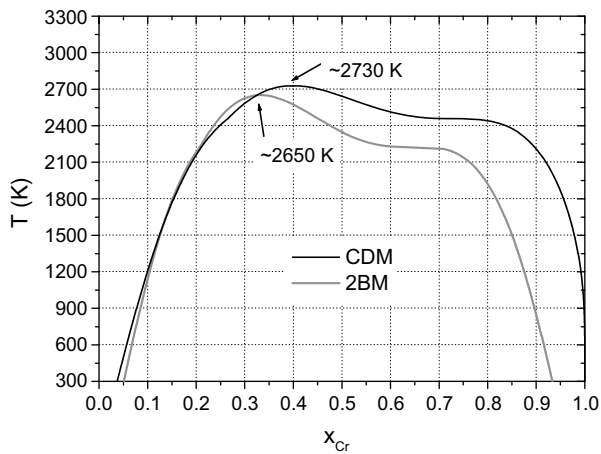
Fig. 8. Phase diagram (α–α′ miscibility gap) according to CDM and 2BM in regular solution approximation. This approximation is adequate for CDM, but not so for 2BM (see text). From [115].

This choice allows the composition of the α′-phase to be correctly predicted at temperatures of technological interest by the 2BM (something that both CDM and CE fail to do [115]), at the price of introducing an arbitrary dependence of the mixing enthalpy on Cr concentration, that is probably not physically.

There is of course, in the case of FeCr alloys, one additional and important 'ingredient' that should be accounted for, in order to reproduce the thermodynamic properties of the system: *magnetism*. It seems reasonable to expect that magnetic entropy will have an impact on the thermodynamic properties, e.g. on the shape of the miscibility gap, especially at high temperature, when approaching the Curie temperature, T_C. It is also in this range where magnetism will have an important effect in determining the stability of low energy structures and, in general, the mixing enthalpy. Then, above T_C, a second order magnetic transition to the paramagnetic state occurs, which of course cannot be allowed for by models such as those analysed here. Explicitly accounting for magnetic effects is therefore likely to be a way of inherently improving the reliability of model hamiltonians. To this regards, Ackland has shown that a simple Ising model hamiltonian, where both spins and species are included as spin-like variables in Monte Carlo simulations on a bcc rigid lattice (with one species, 'Fe', treated as ferromagnetic and the other, 'Cr', as antiferromagnetic) provides, *without fitting*, a phase diagram that is qualitatively very similar to that of FeCr (skewed miscibility gap), including magnetic transitions (Curie and Néel temperatures) [31]. This suggests that an empirical potential formalism explicitly including not only species and distances as variables, but also spins, would be likely to reproduce correctly, with only limited fitting effort, the thermodynamic properties of the FeCr system. Possibly, such an approach may be a way to reproduce also the α -γ transition of pure Fe, already empirically reproduced by Tersoff-like potentials [137]. Nonetheless, we have clearly shown that, even without spin dynamics, the models here analysed do succeed in catching phenomenologically its main effects on the thermodynamic behaviour of FeCr alloys, certainly up to 700 K, a temperature up to which they can thus be reliably used. Above this temperature, too, they perform reasonably well, particularly the 2BM, although their reliability and acceptability is certainly lessened. In addition, magnetism is only one more 'ingredient' to be allowed for, explicitly or implicitly, in a semi-empirical cohesive model. Even a model explicitly including spin dynamics will have to cope with a proper description of the mixing enthalpy at finite temperature, the low energy structures and, above all, the vibrational entropy which,

in the case of FeCr, is clearly one of the main contributors to determining the phase diagram at high temperature [115,136]. Finally, the development of a spin polarised potential requires not only the effort of working out the formalism, but also, and more crucially, of devising a way to treat spin dynamics in, for example, a MD code [35].

5.2. Physical and methodological problems to be addressed to model concentrated FeCr alloys under irradiation

The previous sections clearly indicate that in FeCr the microstructure evolution under irradiation is the consequence of strongly coupled, concomitant phase changes and defect processes that inextricably influence each other. This is of course the case for all materials, but in this system the problem appears particularly involved, one of the reasons being the relatively large solubility limit of Cr in Fe and the fact that two opposite behaviours (ordering and clustering) are simultaneously exhibited. Another reason is the strong interaction between SIA and Cr atoms, which suggests, for example, the possibility that SIA loops may be Cr-enriched and that their stability may depend on that. Even more, there is experimental evidence that radiation-induced α′ precipitation may occur on SIA loops [138]. If true, under irradiation phase transformation may be not only enhanced, but also induced by two opposite reasons, simultaneously involving negligible interaction between Cr and vacancies (with subsequent formation of α′ *away* from voids [2]) and strong interaction between Cr and SIAs (with possible transport of Cr atoms to loops by the latter). Thus, coarse-grained microstructure evolution models based on mean-field rate-theory approaches [131,139] or on the solution of the master equation using kinetic Monte Carlo methods (object KMC, see for example Ref. [123]) should, in principle, contain a proper and coupled treatment of both phenomena. In dilute alloys this is formally possible, up to a certain extent [123,139]. However, in the case of concentrated alloys no self-consistent, fully developed methodology exists, to our knowledge, capable of treating both problems at the same time and effort is certainly needed in this direction. Different paths can be followed towards this goal, but none of them is trivial. Sticking to atomic-level models, the way could be the development of AKMC models where the rigid lattice approximation is removed or at least relaxed. In this case the main difficulty is, aside from the need to treat very large atomic systems (thereby requiring a parallelisation scheme [140]), the evaluation of the transition rates as functions of the local chemical environment and strain field. A number of partial solutions exist currently in the literature [141–143], but as yet none of them has been fully developed and successfully applied to radiation damage. As an alternative, large systems of equations coupling advanced rate theory [131] and, for example, phase field models [144] should be devised. Finite element frameworks potentially capable of managing such a combined model exist [145], but to our knowledge no serious attempt has been made yet to actually apply them to the problem of radiation damage in concentrated alloys. As a short-term alternative, rate theory [131,139] or OKMC [123] models with appropriate effective parameters seem to be the only possibility currently at hand. But even this approach is not easily applied, because of the difficulty of estimating, at the atomic-level, quantities such as formation, binding and migration energies in concentrated alloys, as illustrated in Section 4.2. Efforts to extend our knowledge in this sense are ongoing [146]. There is, however, need for a large, long-term and coordinated research effort in order to reach the goal of developing reliable predictive models for the description of the microstructure evolution under irradiation in concentrated alloys, especially in FeCr alloys.

Another problem that remains open, even at the level of basic understanding and assessment of experimental data, is the non-

monotonic dependence of radiation-induced hardening and embrittlement as functions of Cr concentration in Fe, already outlined in the introduction. In this case, however, even the tools currently available, i.e. the existing interatomic potentials, can be already of help. Molecular dynamics simulations of dislocations mobility and their interaction with given microstructural features are nowadays commonplace [147,148]. Simulations of this type with chosen microstructures are likely to provide at least qualitative answers concerning hardening effects and their dependence on Cr concentration, both in the absence and presence of defects. For example, it has been seen [46] that the presence of Cr atoms, particularly Cr-Cr pairs, may significantly affect kink pair formation on screw dislocations in FeCr alloys, suggesting a strong dependence of dislocation motion on the actual Cr distribution and providing a framework to understand solute softening and hardening experimentally observed in these alloys [149]. The interaction between Cr-rich precipitates in concentrated alloys and edge dislocations has been also studied [47], finding that, in first approximation, it is possible to treat precipitate hardening in the concentrated alloy as the sum of a matrix contribution (friction stress) plus the precipitate contribution, as assessed in a pure Fe matrix. Similar studies including voids and SIA clusters are ongoing [150,151] and are expected to provide input for the development of mesoscopic dislocation dynamics models [152].

It is, however, important to have a starting mechanistic framework for the rationalisation of the experimental results. As mentioned in the introduction, the scarce data concerning radiation-hardening in FeCr alloys versus Cr content are not fully consistent with each other and with radiation-embrittlement data. In particular, while three sets of data [48,52,60,61] seem to be consistent in showing higher radiation-hardening as soon as Cr is added to Fe, with a kind of plateau, followed by increased hardening above 9%Cr, one early set of data [62] suggests linear increase. In addition, embrittlement data suggest a deep minimum at 9%Cr [59], which is not found (so far) in hardening data. Radiation-embrittlement is a complex phenomenon related, among other things, to plastic localisation; it is therefore ambitious to try to rationalize it in terms of qualitative microstructural considerations deduced from atomic-level models. In addition, the validity of the data suggesting the deep radiation-embrittlement minimum at 9%Cr presented in [59] has been recently questioned [153], on the basis of the proven inadequacy of Charpy tests to predict the shift of the ductile-brittle transition temperature under irradiation in ferritic/martensitic steels. According to this argument, Charpy tests would understimate the actual shift when martensite is in the microstructure; as a consequence, the deep minimum should be interpreted in the best case as a shallow minimum [153], thereby providing a better correlation with hardening data, that suggest a plateau instead [48,52,60,61]. If, therefore, we stick to radiation-hardening data, based on the current qualitative understanding of radiation effects in FeCr presented and discussed in the present paper, as well as on experimental indications from the literature on the Cr dependence of the proportion of ½<111> and <100> dislocation population under irradiation [54,55,154], a simplified, mechanistic approach can be proposed, whereby the radiation-hardening, $\Delta\sigma_y$, would be the result of the composition of different contributions:

$$\Delta\sigma_y(\text{FeCr}) = \Delta\sigma_y(\text{Fe}) + \Delta\sigma_y^{\text{SRO}} + \Delta\sigma_y^{\text{invisible}} + \Delta\sigma_y^{\langle 1\,1\,1\rangle/\langle 1\,0\,0\rangle}. \quad (6)$$

Here, $\Delta\sigma_y(\text{Fe})$ represents the hardening in pure Fe, which saturates at relatively low dose and remains, afterwards, essentially constant [60,61]. The other three terms correspond to phenomena that only occur in the presence of Cr and at higher doses, namely: (1) SRO parameter changes ($\Delta\sigma_y^{\text{SRO}}$), allowing for either Cr ordering or clustering (α') depending on temperature and concentration; (2) accumulation of (TEM-)invisible defects ($\Delta\sigma_y^{\text{invisible}}$), most likely – in

the light of the existence of atomic trapping configurations – small interstitial clusters; and (3) effect of a different ratio of $\langle 100\rangle$-to-½$\langle 111\rangle$ loops or dislocations in the developed dislocation network ($\Delta\sigma_y^{111/100}$), a term that could also include the effect of possible changes in the average size of the visible loops, depending on Cr concentration. It is our belief that the accumulation of invisible defects provides the largest contribution to hardening, as compared to pure Fe, particularly at concentrations below 9%. The other two contributions 'modulate' this hardening background. In particular, the zero SRO at 9% may determine the presence of a local minimum of hardening at that concentration, although this minimum may in fact be not the simple effect of the Cr distribution on dislocation motion, but rather the effect of the coupling of order and increased trapping of self-interstitials and their small clusters, as suggested by recent DFT calculations [38]. Precise investigations are needed to confirm or reject these contentions.

6. Summary

In this article, we have reviewed the properties and the behaviour under irradiation of FeCr alloys, bases for the most promising steels for future nuclear applications. Likewise we reviewed the efforts done to model them from *ab initio* electronic theories to empirical potentials. The main source of complexity of this system is the non-monotonic dependence on Cr concentration observed for a number of quantities and properties characterising its thermodynamic behaviour (ordering/clustering) and its response to irradiation (different loop population, increased and modulated hardening and embrittlement, swelling), which is a priori not easy to rationalize. Thermodynamic behaviour and response to irradiation are, on the other hand, inextricably correlated and particularly difficult to model in a concentrated alloy. Nonetheless, recent progress in the theoretical approach at electronic and atomic scales has provided keys to understand several experimental observations regarding ordering, resistivity recovery, precipitation, and swelling in this system. These keys are, in a nutshell, the change of sign of the mixing enthalpy, due to magnetic reasons, and the strong interaction between self-interstitials, especially crowdions, and Cr atoms, with negligible effect of Cr atoms on vacancies. Two interatomic potentials have been developed, based on different approaches, both capable of grasping these features. After a detailed description of their achievements in clarifying a number of issues concerning the behaviour of the FeCr system, as well as their limitations, we have attempted an explanation for the discrepancies still present between predictions and experimental evidence, highlighting the points that require deeper understanding and identifying areas of research that could, even in the short term, allow an even better qualitative understanding of the mechanisms governing the response of FeCr systems to irradiation.

References

[1] E.A. Little, J. Nucl. Mater. 87 (1979) 11.
[2] E.A. Little, D.A. Stow, J. Nucl. Mater. 87 (1979) 25.
[3] E.A. Little, D.A. Stow, J. Metal Sci. 14 (1980) 89.
[4] E.A. Little, R. Bullough, M.H. Wood, Proc. R. Soc. London A 372 (1980) 565.
[5] N. Singh, J.H. Evans, J. Nucl. Mater. 226 (1995) 277.
[6] F.A. Garner, M.B. Toloczko, B.H. Sencer, J. Nucl. Mater. 276 (2000) 123.
[7] A. Fry, S. Osgerby, M. Wright, Oxidation of alloys in steam environment – a review, National Physics Laboratory Report NPL MATC(A)90, September, 2002.
[8] R.L. Klueh, D.R. Harries, High-Chromium Ferritic and Martensitic Steels for Nuclear Applications, ASTM Monograph 3, American Society for Testing and Materials, West Conshohocken, PA, 2001.
[9] L.K. Mansur, A.F. Rowcliffe, R.K. Nanstad, S.J. Zinkle, W.R. Corwin, R.E. Stoller, J. Nucl. Mater. 329–333 (2004) 166.
[10] R.L. Klueh, A.T. Nelson, J. Nucl. Mater. 371 (2007) 37.
[11] S.J. Zinkle, Phys. Plasmas 12 (2005) 058101.
[12] P. Olsson, I.A. Abrikosov, L. Vitos, J. Wallenius, J. Nucl. Mater. 321 (2003) 84.
[13] P. Olsson, L. Malerba, A. Almazouzi, SCK•CEN Scientific Report BLG-950, June, 2003.
[14] L. Malerba, D.A. Terentyev, P. Olsson, R. Chakarova, J. Wallenius, J. Nucl. Mater. 329–333 (2004) 1156.
[15] D. Terentyev, L. Malerba, J. Nucl. Mater. 329–333 (2004) 1161.
[16] J. Wallenius, I.A. Abrikosov, R. Chakarova, C. Lagerstedt, L. Malerba, P. Olsson, V. Pontikis, N. Sandberg, D. Terentyev, J. Nucl. Mater. 329–333 (2004) 1175.
[17] J. Wallenius, P. Olsson, C. Lagerstedt, N. Sandberg, R. Chalarova, V. Pontikis, Phys. Rev. B 69 (2004) 094103.
[18] D. Terentyev, L. Malerba, M. Hou, Nucl. Instrum. and Meth. B 228 (2005) 156.
[19] D.A. Terentyev, L. Malerba, A.V. Barashev, Philos. Mag. Lett. 85 (11) (2005) 587.
[20] A. Caro, D.A. Crowson, M. Caro, Phys. Rev. Lett. 95 (2005) 075702.
[21] P. Olsson, J. Wallenius, C. Domain, K. Nordlund, L. Malerba, Phys. Rev. B 72 (2005) 214119.
[22] P. Olsson, Modelling of formation and evolution of defects and precipitates in Fe–Cr alloys of reactor relevance, Ph.D. dissertation, Uppsala University, 2005.
[23] D.A. Terentyev, L. Malerba, R. Chakarova, K. Nordlund, P. Olsson, M. Rieth, J. Wallenius, J. Nucl. Mater. 349 (2006) 119.
[24] D.A. Terentyev, Study of radiation effects in FeCr alloys for fusion applications using computer simulations, Ph.D. dissertation, Free University of Brussels, 2006. <http://www.sckcen.be/sckcen_en/publications/theses/PhD_Terentyev_v3_06112006.pdf>.
[25] D.A. Terentyev, L. Malerba, SCK CEN Scientific Report BLG-1026, June, 2006.
[26] P. Olsson, I.A. Abrikosov, J. Wallenius, Phys. Rev. B 73 (2006) 104416.
[27] T.P.C. Klaver, R. Drautz, M.W. Finnis, Phys. Rev. B 74 (2006) 094435.
[28] J.-H. Shim, H.-J. Lee, B.D. Wirth, J. Nucl. Mater. 351 (2006) 56.
[29] A. Caro, M. Caro, E.M. Lopasso, D. Crowson, Appl. Phys. Lett. 89 (2006) 121902.
[30] (a) L. Malerba, SCK CEN External Report ER-16, June, 2006;
    (b) G. Bonny, D. Terentyev, L. Malerba, Scripta Mater. (2008), doi:10.1016/j.scriptamat.2008.08.008.
[31] G.J. Ackland, Phys. Rev. Lett. 97 (2006) 015502.
[32] P. Olsson, C. Domain, J. Wallenius, Phys. Rev. B 75 (2007) 014110.
[33] M.Yu. Lavrentiev, R. Drautz, D. Nguyen-Mahn, T.P.C. Klaver, S.L. Dudarev, Phys. Rev. B 75 (2007) 014208.
[34] D. Terentyev, P. Olsson, L. Malerba, A.V. Barashev, J. Nucl. Mater. 362 (2007) 167.
[35] J. Wallenius, P. Olsson, L. Malerba, D. Terentyev, Nucl. Instrum. and Meth. B 255 (2007) 68.
[36] A. Caro, M. Caro, T.P.C. Klaver, B. Sadigh, E.M. Lopasso, S.G. Srinivasan, TMS JOM 59 (2007) 50.
[37] L. Malerba, G. Bonny, D.A. Terentyev, A.V. Barashev, C. Björkas, N. Juslin, K. Nordlund, C. Domain, P. Olsson, N. Sandberg, J. Wallenius, J. ASTM Intl. 4 (2007) JAI100692.
[38] T.P.C. Klaver, P. Olsson, M.W. Finnis, Phys. Rev. B 76 (2007) 214110.
[39] A. Froideval, R. Iglesias, M. Samaras, S. Schuppler, P. Nagel, D. Grolimund, M. Victoria, W. Hoffelner, Phys. Rev. Lett. 99 (2007) 237201.
[40] P. Erhart, B. Sadigh, A. Caro, Appl. Phys. Lett. 92 (2008) 141904.
[41] P. Erhart, A. Caro, M. Serrano de Caro, B. Sadigh, Phys. Rev. B 77 (2008) 134206.
[42] D. Terentyev, L. Malerba, A.V. Barashev, Philos. Mag. 88 (2008) 21.
[43] G. Bonny, D. Terentyev, L. Malerba, Comput. Mater. Sci. 42 (2008) 107.
[44] C. Björkas, K. Nordlund, L. Malerba, D. Terentyev, P. Olsson, J. Nucl. Mater. 372 (2008) 312.
[45] D. Terentyev, P. Olsson, T.P.C. Klaver, L. Malerba, Comput. Mater. Sci. (2008), doi:10.1016/j.commatsci.2008.03.013.
[46] D.A. Terentyev, L. Malerba, Comput. Mater. Sci. (2008), doi:10.1016/j.commatsci.2008.01.072.
[47] D.A. Terentyev, G. Bonny, L. Malerba, Acta Mater. (2008), doi:10.1016/j.actamat.2008.03.004.
[48] A. Okada, N. Kawaguchi, M.L. Hamilton, K. Hamada, T. Yoshiie, I. Ishida, E. Hirota, J. Nucl. Mater. 212–215 (1994) 382.
[49] A. Okada, H. Maeda, K. Hamada, I. Ishida, J. Nucl. Mater. 271&272 (1999) 133.
[50] N. Yoshida, A. Yamaguchi, T. Muroga, Y. Miyamoto, K. Kitajima, J. Nucl. Mater. 155–157 (1988) 1232.
[51] K. Arakawa, M. Hatanaka, H. Mori, K. Ono, J. Nucl. Mater. 329–333 (2004) 1194.
[52] S.I. Porollo, A.M. Dvoriashin, A.N. Vorobyev, Yu.V. Konobeev, J. Nucl. Mater. 256 (1998) 247.
[53] Yu.V. Konobeev, A.M. Dvoriashin, S.I. Porollo, F.A. Garner, J. Nucl. Mater. 355 (2006) 124.
[54] D.S. Gelles, J. Nucl. Mater. 108&109 (1982) 515.
[55] Y. Katoh, A. Kohyama, D.S. Gelles, J. Nucl. Mater. 225 (1995) 154.
[56] D.S. Gelles, J. Nucl. Mater. 225 (1995) 163.
[57] N.I. Budylkin, E.G. Mironova, V.M. Chernov, V.A. Krasnoselov, S.I. Porollo, F.A. Garner, J. Nucl. Mater. 375 (2008) 359.
[58] H. Kayano, A. Kimura, M. Narui, Y. Sasaki, Y. Suzuki, S. Ohta, J. Nucl. Mater. 155–157 (1988) 978.
[59] A. Kohyama, A. Hishinuma, D.S. Gelles, R.L. Klueh, W. Dietz, K. Ehrlich, J. Nucl. Mater. 233–237 (1996) 138.
[60] M. Matijasevic, A. Almazouzi, in: Structural and Refractory Materials for Fusion and Fission Technologies, MRS Proceedings 981E (2006) 0981-JJ07-06.
[61] M. Matijasevic, A. Almazouzi, J. Nucl. Mater. (2008), doi:10.1016/j;jnucmat2008.02.061.
[62] (a) K. Suganuma, H. Kayano, S. Yajima, J. Nucl. Mater. 105 (1982) 23;
    (b) K. Suganuma, H. Kayano, J. Nucl. Mater. 118 (1983) 234.
[63] P. Dubuisson, D. Gilbon, J.L. Séran, J. Nucl. Mater. 205 (1993) 178.
[64] M.H. Mathon, Y. de Carlan, G. Geoffroy, X. Averty, C.H. de Novion, A. Alamo, in: S.T. Rosinski, M.L. Grossbeck, T.R. Allen, A.S. Kumar, (Eds.), Effects of Radiation on Materials: 20th International Symposium, ASTM STP 1405, American Society for Testing and Materials, West Conshohocken, PA, 2001, p. 674.
[65] M.H. Mathon, Y. de Carlan, G. Geoffroy, X. Averty, A. Alamo, C.H. de Novion, J. Nucl. Mater. 312 (2003) 236.
[66] M.H. Mathon, Y. de Carlan, X. Averty, A. Alamo, C.H. de Novion, J. ASTM Int. 2 (2005) JAI12381.
[67] J.J. Heger, Metal Prog. (1951) 55.
[68] R.M. Fisher, E.J. Dulis, K.G. Carroll, J. Metal: Trans. Am. Inst. Min. Met. Eng. 197 (1953) 690.
[69] (a) R.O. Williams, H.W. Paxton, J. Brit. Iron & Steel Inst. 185 (1957) 358;
    (b) R.O. Williams, Trans. Met. Soc. Am. Inst. Min. Met. Eng. 212 (1958) 497.
[70] R. Lagneborg, Trans. ASM 60 (1967) 67–78.
[71] P.J. Grobner, Metall. Trans. 4 (1973) 251–260.
[72] P. Jacobsson, Y. Bergström, B. Aronsson, Metall. Trans. 6A (1977) 1577.
[73] I. Mirebeau, M. Hennion, G. Parette, Phys. Rev. Lett. 53 (1984) 687.
[74] N.P. Filippova, V.A. Shabashov, A.L. Nikolaev, Phys. Met. Metall. 90 (2000) 145.
[75] V.V. Sagaradze, I.I. Kositsyna, V.L. Arbuzov, V.A. Shabashov, Yu.I. Filippov, Phys. Met. Metall. 92 (2001) 89.
[76] A.A. Mirzoev, M.M. Yalalov, D.A. Mirzaev, Phys. Met. Metall. 97 (2004) 336.
[77] D. Nguyen-Mahn, M.Yu. Lavrentiev, S.L. Dudarev, in: P. Gumbsch (Ed.), Proceedings of the Third International Conference on Multiscale Materials Modelling, Fraunhofer IRB Verlag, Freiburg, Germany, 2006, p. 767.
[78] R. Hafner, D. Spišák, R. Lorenz, J. Hafner, J. Phys.: Condens. Mat. 13 (2001) L239.
[79] D. Nguyen-Manh, M.Yu. Lavrentiev, S.L. Dudarev, C.R. Phys. 9 (2008) 379.
[80] T.B. Massalsky, H. Okamoto, P.R. Subramanian, L. Kacprzac (Eds.), Binary Alloy Phase Diagrams, vol. 1273, ASM International, 1990.
[81] J.-O. Andersson, B. Sundman, CALPHAD 11 (1987) 83.
[82] N. Saunders, P. Miodownik, in: R.W. Cahn (Ed.), Calphad: A Comprehensive Guide, Pergamon Materials Series, 1998.
[83] H. Kuwano, Trans. Jpn. Inst. Met. 26 (2) (1985) 473.
[84] H. Kuwano, Y. Hamaguchi, J. Nucl. Mater. 155–157 (1988) 1071.
[85] F. Danoix, P. Auger, Mater. Character 44 (2000) 177.
[86] S.S. Brenner, M.K. Miller, W.A. Soffa, Scripta Metall. 16 (1982) 831.
[87] S.M. Dubiel, G. Inden, Z. Metallkde. 78 (8) (1987) 544.
[88] P. Olsson, Proceedings of ICFRM13, J. Nucl. Mater., accepted for publication.
[89] F. Maury, P. Lucasson, A. Lucasson, F. Faudot, J. Bigot, J. Phys. F: Met. Phys. 17 (1987) 1143.
[90] H. Abe, E. Kuramoto, J. Nucl. Mater. 271&272 (1999) 209.
[91] (a) A.L. Nikolaev, V.L. Arbuzov, A.E. Davletshin, J. Phys.: Condens. Mat. 9 (1997) 4385;
    (b) A.L. Nikolaev, J. Phys.: Condens. Mat. 11 (1999) 8633;
    (c) A.L. Nikolaev, Philos. Mag. 87 (2007) 4847.
[92] A. Benkaddour, C. Dimitrov, O. Dimitrov, Mater. Sci. Forum 15–18 (1987) 1263.
[93] C. Dimitrov, A. Benkaddour, C. Corbel, P. Moser, Ann. Chim. Fr. 16 (1991) 319.
[94] C. Demangeat, Philos. Mag. 32 (1975) 323.
[95] A. Möslang, E. Albert, E. Recknagel, A. Weidinger, Hyperfine Interact. 15/16 (1983) 409.
[96] E. Kuramoto, S. Nagano, K. Nishi, K. Makii, Y. Aono, M. Takenaka, Mater. Sci. Forum 105–110 (1992) 1125.
[97] R.A. Wolfe, H.W. Paxton, Trans. Metall. Soc. AIME 230 (1964) 1426.
[98] A.M. Huntz, P. Guiraldenq, M. Aucouturier, P. Lacombe, Mém. Sci. Rev. Métall. LXVI (1969) 85.
[99] A.W. Bowen, G.M. Leak, Metall. Trans. 1 (1970) 2767.
[100] R. Braun, M. Feller-Kniepmeier, Phys. Stat. Sol. (a) 90 (1985) 553.

[101] C. Domain, C.S. Becquart, Phys. Rev. B 65 (2001) 024103.
[102] C.-C. Fu, F. Willaime, P. Ordejón, Phys. Rev. Lett. 92 (2004) 175503.
[103] D.A. Terentyev, L. Malerba, M. Hou, Phys. Rev. B 75 (2007) 104108.
[104] Yu.N. Osetsky, D.J. Bacon, A. Serra, B.N. Singh, S.I. Golubov, Philos. Mag. 83 (2003) 61.
[105] A. Caro, P.E.A. Turchi, M. Caro, E.M. Lopasso, J. Nucl. Mater. 336 (2005) 233.
[106] M. Daw, M.I. Baskes, Phys. Rev. B 29 (1984) 6443.
[107] M.W. Finnis, J.E. Sinclair, Philos. Mag. A 50 (1984) 45.
[108] G.J. Ackland, M.I. Mendelev, D.J. Srlolovitz, S. Han, A.V. Barashev, J. Phys. Condens. Mat. 16 (2004) 1.
[109] M.I. Mendelev, S.W. Han, D.J. Srolovitz, G.J. Ackland, D.Y. Sun, M. Asta, Philos. Mag. A 83 (2003) 3977.
[110] O. Redlich, A.T. Kister, Ind. Eng. Chem. 40 (1948) 345.
[111] G.J. Ackland, S.K. Reed, Phys. Rev. B 67 (2003) 174108.
[112] G. Kresse, J. Hafner, Phys. Rev. B 47 (1993) 558.
[113] G. Kresse, J. Furthmüller, Phys. Rev. B 54 (1996) 11169.
[114] G. Kresse, J. Furthmüller, Comput. Mater. Sci. 6 (1996) 15.
[115] G. Bonny, R.C. Pasianot, L. Malerba, A. Caro, P. Olsson, M. Lavrentiev, Proceedings of E-MRS Spring 2008, Symposium N, J. Nucl. Mater., accepted for publication.
[116] J.M. Sanchez, F. Ducastelle, D. Gratias, Physica A 128 (1984) 334.
[117] K. Binder, in: K. Binder (Ed.), Monte Carlo Methods in Statistical Physics, Springer Verlag, Berlin, 1979, p. 1 (Chapter 1).
[118] N. Metropolis, A.W. Rosenbluth, M.N. Rosenbluth, A.H. Teller, E. Teller, J. Chem. Phys. 21 (1953) 1087.
[119] B. Sadigh, A. Caro, some information can be found in Ref. [36].
[120] K.A. Fichthorn, W.H. Weinberg, J. Chem. Phys. 95 (1991) 1090.
[121] F. Soisson, J. Nucl. Mater. 349 (2006) 235.
[122] C. Domain, C.S. Becquart, J.C. Van Duysen, MRS Proceedings 540 (1999) 643.
[123] C. Domain, C.S. Becquart, L. Malerba, J. Nucl. Mater. 335 (2004) 121.
[124] A. Davies, J.A. Stroscio, D.T. Pierce, R.J. Celotta, Phys. Rev. Lett. 76 (1996) 4175.
[125] W.T. Geng, Phys. Rev. B 68 (2003) 233402.
[126] Yu.N. Osetsky, Def. & Diff. Forum 188–190 (2001) 71.
[127] L. Malerba, J. Nucl. Mater. 351 (2006) 28.
[128] S.L. Dudarev, Phys. Rev. B 65 (2002) 224105.
[129] L.A. Zepeda-Ruiz, J. Rottler, B.D. Wirth, R. Car, D.J. Srolovitz, Acta Mater. 53 (2005) 1985.
[130] B.N. Singh, S.I. Golubov, H. Trinkaus, A. Serra, Yu.N. Osetsky, A.V. Barashev, J. Nucl. Mater. 251 (1997) 107.
[131] S.I. Golubov, B.N. Singh, H. Trinkaus, J. Nucl. Mater. 276 (2000) 78.
[132] E. Ogando Arregui, M. Caro, A. Caro, Phys. Rev. B 66 (2002) 054201.
[133] E.M. Lopasso, M. Caro, A. Caro, P.E.A. Turchi, Phys. Rev. B 68 (2003) 214205.
[134] A. Caro, M. Caro, E.M. Lopasso, P.E.A. Turchi, D. Farkas, J. Nucl. Mater. 349 (2006) 317.
[135] G. Bonny, P. Erhart, A. Caro, R.C. Pasianot, L. Malerba, M. Caro, Model. Simul. Mater. Sci. Eng., submitted for publication.
[136] B. Fultz, L. Anthony, J.L. Robertson, R.M. Nicklow, S. Spooner, M. Mostoller, Phys. Rev. B 52 (1995) 3280.
[137] M. Müller, P. Erhart, K. Albe, J. Phys.: Condens. Mat. 19 (2007) 326220.
[138] (a) E. Wakai, A. Hishinuma, Y. Kato, H. Yano, S. Takaki, K. Abiko, J. Phys. IV, Coll. C7, Suppl. J. Phys. III 5 (1995) 277;
(b) E. Wakai, A. Hishinuma, K. Usami, Y. Kato, S. Takaki, K. Abiko, Mater. Trans. JIM 41 (2000) 1180.
[139] F. Christien, A. Barbu, J. Nucl. Mater. 324 (2004) 90.
[140] E. Martínez, J. Marian, M.H. Kalos, J.M. Perlado, J. Comput. Phys. 277 (2008) 3804.
[141] D.R. Mason, T.S. Hudson, A.P. Sutton, Comput. Phys. Commun. 165 (2005) 37.
[142] K. Sastry, D.D. Johnson, D.E. Goldberg, P. Bellon, Phys. Rev. B 72 (2005) 085438.
[143] F.G. Djurabekova, R. Domingos, G. Cerchiara, N. Castin, E. Vincent, L. Malerba, Nucl. Instrum. and Meth. B 255 (2007) 8.
[144] A. Badillo, Y. Liu, P. Krasnochtchekov, R.S. Averback, P. Bellon, in: P. Gumbsch (Ed.), Proceedings of the Third International Conference on Multiscale Materials Modeling, Fraunhofer IRB Verlag, Freiburg, Germany, 2006, p. 679.
[145] W.B.J. Zimmerman, Multiphysics Modelling with the Finite Element Methods, World Scientific Publishing Co. Pte. Ltd., Singapore, 2006.
[146] D. Terentyev, P. Olsson, L. Malerba, Proceedings ICFRM-13, J. Nucl. Mater., accepted for publication.
[147] D.J. Bacon, Yu.N. Osetsky, Mater. Sci. Eng. A 400–401 (2005) 353.
[148] C. Domain, G. Monnet, Phys. Rev. Lett. 95 (2005) 215506.
[149] (a) R. Stephens, W.R. Witzke, J. Less-Commun. Metals 48 (1976) 285;
(b) M.J. Kelley, N.S. Stoloff, Metall. Trans. A 7 (1976) 331.
[150] D. Terentyev, G. Bonny, L. Malerba, Proceedings ICFRM-13, J. Nucl. Mater., accepted for publication.
[151] G. Bonny, D. Terentyev, L. Malerba, Proceedings E-MRS Spring 2008, Symposium N, J. Nucl. Mater., accepted for publication.
[152] (a) Gh. Monnet, Acta Mater. 55 (2007) 5081;
(b) S. Queyreau, Gh. Monnet, B. Devincre, Intl. J. Plast. (2008), doi:10.1016/j.ijplas.2007.12.009.
[153] R. Chaouadi, J. Nucl. Mater. 360 (2007) 75.
[154] D.S. Gelles, in: Effects of Radiation on Materials: 14th International Symposium, vol. 1, ASTM STP 1046, N.H. Packan, R.E. Stoller, A.S. Kumar (Eds.), American Society for Testing and Materials, Philadelphia, 1989, p. 73.